JOURNAL OF GEOPHYSICAL RESEARCH, VOL. 114, D12110, doi:10.1029/2008JD011217, 2009

Model-based constraints on interpreting 20th century trends in ice core ^{10}Be

Christy V. Field[1,2] and Gavin A. Schmidt[2,3]

Received 29 September 2008; revised 16 April 2009; accepted 29 April 2009; published 20 June 2009.

[1] Beryllium-10 ice-core records are useful for understanding solar magnetic field changes over time, and in particular over the 20th century, during which there are a variety of relevant observations. However, differences between ^{10}Be snow concentration records from different locations complicate the process of developing a coherent understanding of changes in cosmogenic isotope production. We use the Goddard Institute for Space Studies ModelE general circulation model to simulate the production and transport of beryllium isotopes for this time period. We compare our results with surface air observations, and with ice-core records from Dye 3, Taylor Dome, and South Pole. We find that unforced weather-related (internal) variability causes modeled trends in ^{10}Be snow concentration to vary from the ensemble mean by 50% and greater at all three ice-core locations. Lower levels of internal variability at Taylor Dome and South Pole relative to Dye 3 make the simulated ^{10}Be values at these locations better estimates of the ensemble-mean trend in ^{10}Be snow concentration. In addition, the ensemble mean concentration trend at Dye 3 was significantly different from the expected modeled trend based on applied production changes alone. Overall, the results imply that during the 20th century, ^{10}Be data from multiple cores are likely to be required to make meaningful inferences about ^{10}Be production changes. The model simulations imply that data from Antarctica are likely to be more robust.

Citation: Field, C. V., and G. A. Schmidt (2009), Model-based constraints on interpreting 20th century trends in ice core ^{10}Be, *J. Geophys. Res.*, *114*, D12110, doi:10.1029/2008JD011217.

1. Introduction

[2] Understanding the effect of changes in the sun's activity is an important part of understanding Earth's climate variability, particularly if we want to be able to accurately quantify the effects of anthropogenic climate change relative to natural variations. Cosmogenic isotopes can play a key role in this effort, since their production is linked to variations in solar magnetic activity. These changes, which affect the degree to which Earth's atmosphere is shielded from galactic cosmic rays (GCR), are correlated with changes in total solar irradiance (TSI) [*Lean*, 1994; *Lean et al.*, 2002], and have strong 11-year cycles (also known as Schwabe cycles). Increased numbers of sunspots result in both increased TSI and higher levels of GCR shielding (and vice versa during sunspot minima). The physical relationship between this time-varying solar GCR shielding (usually described by the solar modulation parameter ϕ [*Gleeson and Axford*, 1968]) and sunspot activity is still not completely understood [*Mursula et al.*, 2003]. However, the magnitude of ϕ is inversely proportional to the rate of cosmogenic isotope production, hence the usefulness of these isotopes as proxies for changes in TSI.

[3] Two isotopes in particular, beryllium-10 and beryllium-7, are especially useful in this regard. The amplitude of ^{7}Be's production changes is somewhat larger than that for ^{10}Be, and there are also differences between the three-dimensional structures of their production functions, with the ^{7}Be/^{10}Be production ratio varying from about 1.2 at sea level to about 2.6 at the top of the atmosphere (for ϕ = 600 MV). However, the fact that ^{7}Be and ^{10}Be share the same transport and removal processes makes analysis of the former a useful adjunct for understanding the latter. After production in the stratosphere and troposphere, ^{10}Be and ^{7}Be attach to sulfate aerosols and are deposited at the surface after 1–2 years in the global mean, but with a larger range depending on altitude. Beryllium-10's relatively long half-life (1.5 million years) makes it ideal for study on decadal to millennial timescales, and ice-core records provide a rich natural archive for this purpose. While ^{7}Be's 53-day half-life makes it unsuitable for ice-core study, it is much easier to measure, and its concentrations in air are often recorded as part of standard radiation monitoring programs (Environmental Measurement Laboratory Surface Air Sampling Program database available at http://www.eml.doe.gov).

[1]Department of Earth and Environmental Sciences, Columbia University, New York, New York, USA.
[2]NASA Goddard Institute for Space Studies, New York, New York, USA.
[3]Center for Climate Systems Research, Columbia University, New York, New York, USA.

0148-0227/09/2008JD011217$09.00

[4] Technological developments have made it possible to infer ϕ values, either from neutron monitor data, ionization chamber data, or various cosmogenic nuclides, over most of the 20th century [*Beer*, 2000; *McCracken and Heikkila*, 2003]. These can be compared with various ^{10}Be ice-core observations from the same time period. However, ^{10}Be snow concentrations from different ice cores [*Beer et al.*, 1990; *Raisbeck et al.*, 1990; *Steig et al.*, 1996; *Vonmoos et al.*, 2006] often exhibit different features, trends and amplitudes [*Bard et al.*, 1997, 2007; *Muscheler et al.*, 2007a, 2007b]. These discrepancies have led to debate over which ^{10}Be records most accurately reflect changes in ϕ, and by extension, changes in TSI.

[5] General circulation models, with their ability to control climate forcings and cosmogenic isotope production, provide a means for studying these questions. To better understand the relationship between ϕ and records of ^{10}Be from different ice cores, we perform ensemble runs to simulate 20th century climate forced with transient changes in sea surface temperatures, TSI, ^{10}Be and ^{7}Be production, and atmospheric composition. We then look at how the model results compare with recent surface air observations and 20th century ice-core records, as well as trends in production and snow concentration at different locations.

2. Model Description and Experimental Design

[6] Our experiments were performed using the stratospheric version of the Goddard Institute for Space Studies (GISS) ModelE general circulation model (GCM) [*Schmidt et al.*, 2006], which has a horizontal resolution of 4° × 5° (latitude × longitude), 23 vertical layers, and a model top at 0.002 mb. Having the capability to simulate the full stratosphere is important as approximately half of all ^{10}Be is produced in the stratosphere, and the rate of stratosphere-troposphere exchange is crucial for simulating the correct atmospheric residence time. It is also possible for stratosphere-troposphere exchange to be influenced to some extent by solar activity [*Heikkilä et al.*, 2008]. The formulation for the gravity wave drag is slightly changed from *Schmidt et al.* [2006] to allow for improved stratospheric circulation and stratosphere-troposphere exchange (D. Rind, personal communication, 2008). The age of the model's stratospheric air is well simulated in comparison to other GCMs [*Shindell et al.*, 2006b], although it is somewhat younger than observed values [*Rind et al.*, 2007].

[7] We assume that the beryllium isotopes attach to sulfate aerosols immediately after production, and that there are always sufficient sulfate aerosols available to scavenge them. Beryllium-bearing aerosols are assumed to be 100% soluble. Aerosol gravitational settling is included, and in stratiform and convective clouds, aerosol species are transported, dissolved, evaporated and scavenged according to processes for each cloud type [*Koch et al.*, 2006]. All tracers in the model (including ^{10}Be) are subject to the advection, mixing and convection processes consistent with the modeled air mass fluxes. The model also allows aerosols to settle more quickly in the stratosphere, where the mean free path exceeds the particle radius [*Koch and Rind*, 1998].

[8] The dry deposition scheme is formulated according to *Wesely et al.* [1985] and *Hicks et al.* [1989] as described by *Balkanski et al.* [1993], and uses the resistance-in-series scheme described by *Wesely and Hicks* [1977] (derived from the Harvard GISS chemical transport model [e.g., *Chin et al.*, 1996]). This deposition scheme makes use of the GCM-assumed leaf area indices, surface types, radiation, boundary layer height, Monin-Obhukov length, etc. [*Koch et al.*, 2006; *Wesely*, 1989]. The turbulent exchange coefficients as the model humidity are also used for ^{10}Be in the boundary conditions near the surface.

[9] To simulate the 20th century, we performed two ensembles, each with five runs. In the first ensemble, we used a preindustrial atmospheric composition and forced the model only with time-varying 20th century sea surface temperature (SST) and sea ice values. In the second ensemble, we included a comprehensive set of forcings: changing atmospheric composition, transient volcanic eruptions, prescribed SST and sea ice values, and annually varying solar irradiance with parameterized ozone response [*Shindell et al.*, 2006a]. In both ensembles, we allowed ^{10}Be production to vary annually, based on the reconstructed ϕ values from *Muscheler et al.* [2007b] (Figure 1). The ϕ values are based on ^{14}C data, balloon-borne neutron monitor data, and the geomagnetic reconstruction from *Yang et al.* [2000]. For the cosmogenic isotopes, we used a newer version of the *Masarik and Beer* [1999] production scheme (J. Beer, personal communication, 2007). This updated version more accurately simulates the latitude-dependent production of beryllium isotopes by helium nuclei (alpha particles), which make up about 9% of the GCR particles responsible for ^{10}Be production [*Masarik and Beer*, 1999; *Field et al.*, 2006]. The new production scheme results in levels of production that are about 10% higher than those using the earlier version. For all simulations, the model was run from 1880 to 2000. We used the first 20 years of each simulation to allow atmospheric ^{10}Be concentrations to reach a state of relative equilibrium, and the results shown in this paper are based on the data from 1900 to 2000.

3. Evaluation With Surface-Air Data

[10] To evaluate how the model simulates beryllium isotopes under 20th century circumstances, we compared the model output with time series measurements of ^{7}Be air concentration from the Environmental Measurements Laboratory's Surface Air Sampling Project (SASP). We compare modeled ^{7}Be with measurements from 16 SASP stations that have at least 20 years of data. Results for the runs with only SST forcings (not shown) were very similar to those for the simulations with the full set of climate forcings (shown in Figure 2). In an earlier set of ModelE experiments, *Koch et al.* [2006] found that low-latitude locations tended to have low modeled values of ^{7}Be relative to the observations, with better performance at mid- and high latitudes. Similarly, in our experiments the low-latitude model values are lower than the corresponding observed values, however the same is also usually true for the data at midlatitude and polar locations. The overall low bias may be caused by the production function, which, at 0.035 atoms/cm^2/s, is low relative to some estimates (such as 0.0810 atoms/cm^2/s [*Lal and Peters*, 1967], 0.0578 atoms/cm^2/s [*O'Brien et al.*, 1978] and 0.062 atoms/cm^2/s [*Usoskin and Kovaltsov*, 2008]) but higher compared to the estimates of *Oeschger et al.* [1969] (0.0185 atoms/cm^2/s) and *Masarik and Reedy* [1995]

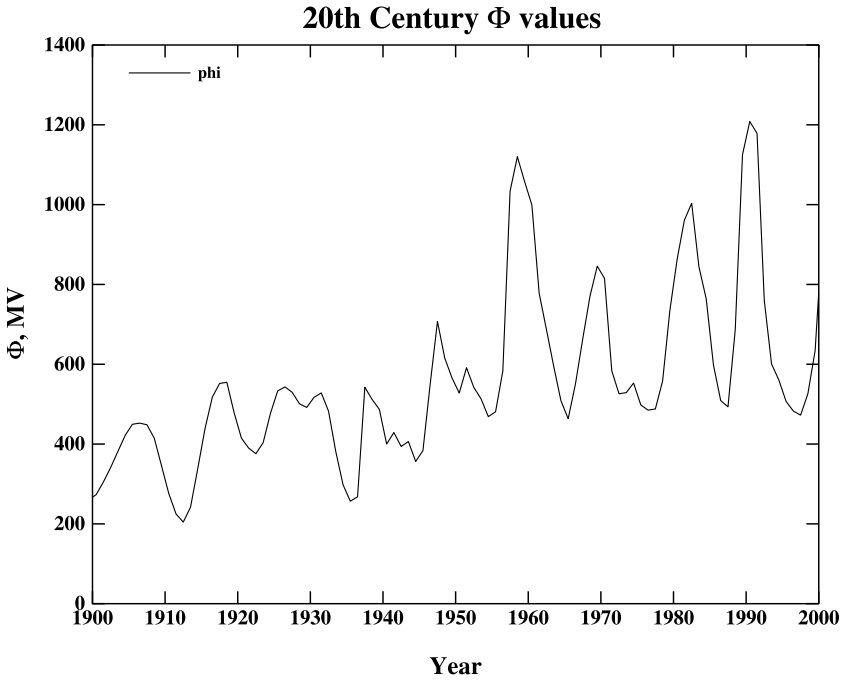

Figure 1. 20th century estimated ϕ values (derived from ^{14}C data and neutron monitors) used in the model to drive beryllium isotope production (data from *Muscheler et al.* [2007b]).

(0.0129 atoms/cm^2/s). (A more comprehensive discussion of the different production functions is given by *Masarik and Beer* [1999] and *Usoskin and Kovaltsov* [2008].) If the mean global ^{7}Be production rate used in our simulations were too low, then we would also expect production values for ^{10}Be to be too low; however, as is discussed in the following section, the opposite (high ^{10}Be relative to the observations) is in fact the case. It is also possible that there may be a problem with the nuclear cross sections used in the production function, or that the model may remove ^{7}Be from surface air too efficiently.

[11] Figure 3 shows the observations as time series, at six representative locations, compared with model results for the simulations with the full set of climate forcings. To better illustrate how the model performs despite the bias toward low values, the time series plots show variability in terms of percent change from the long-term mean, with the seasonal cycle removed. Solar maxima occurred approximately at 1969, 1980, and 1990, and solar minima occurred approximately at 1977, 1987, and 1996; therefore we would expect to see respectively low and high ^{7}Be concentrations immediately after those years. These solar-cycle–related concentration changes tend not to be as clearly defined at low-latitude locations (like Peru) as they generally are at midlatitude locations (like Canada and New York). This is expected because of the higher degree of GCR shielding at low latitudes (and because of the lower levels of shielding, and therefore greater sensitivity of ^{7}Be production to solar modulation changes, at mid- and high latitudes). While the model does a good job of simulating the relative magnitude of the production-related ^{7}Be concentration changes at midlatitudes, it is less successful in capturing the more extreme variability that is evident in the high-latitude observations. It is also possible that higher levels of observed variability near the poles may be related to increased ^{7}Be production from low-energy solar particles. These particles can enter the atmosphere more easily at high latitudes, where magnetic shielding is weaker, and are associated with the solar flares that often characterize the

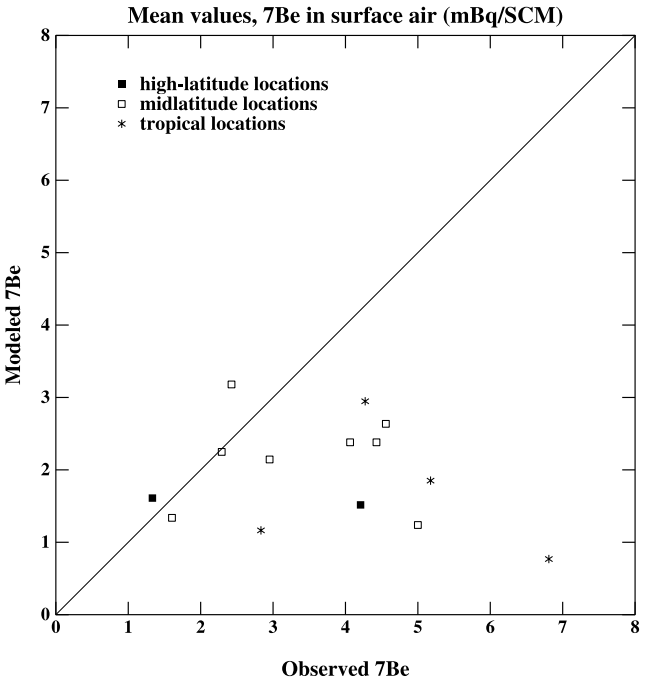

Figure 2. Average values for ^{7}Be air concentrations at SASP locations, except for the Peru, Lima site for clarity (observed value: 13.34 mBq/standard cubic meter; model value: 0.98 mBq/standard cubic meter; 1 Becquerel = 1 nuclear decay per second).

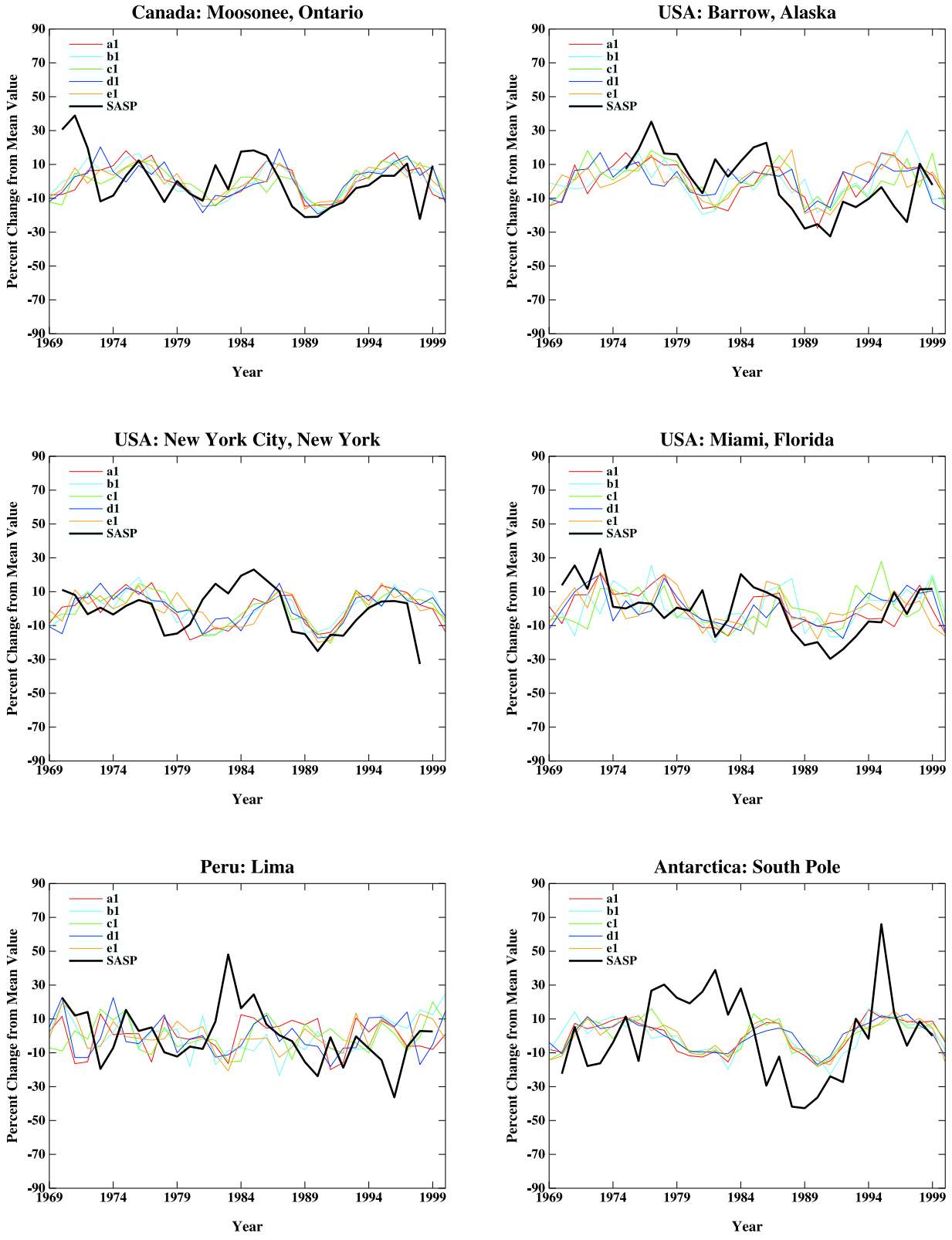

Figure 3. ^{7}Be air concentrations at SASP locations: variability in terms of percent change from the long-term mean, with the seasonal cycle removed. The colored lines show the results for the different ensemble members, and the black line shows the observations.

Table 1. Average ^{10}Be Snow Concentrations ±1 Standard Deviation[a]

Data	Dye 3	Taylor Dome	South Pole
Observations	0.79 ± 0.15	1.77 ± 0.48	3.36 ± 0.42
All forcings	1.25 ± 0.19	2.55 ± 0.34	11.34 ± 1.36
SST forcing only	1.19 ± 0.18	2.51 ± 0.33	11.24 ± 1.57

[a]Modeled values are ensemble averages. Units are 10^4 atoms/g water. Note: the estimates of the standard deviations are relative to the different time resolutions for the three data sets; the standard deviations for the modeled data also take these resolution differences into account.

descending limb of the solar cycle, though it remains unclear how large an effect these particles could have on tropospheric ^{7}Be concentrations [*Lal and Peters*, 1967; *Koch and Mann*, 1996]. Overall, however, the model does a fairly good job of reproducing the variability of ^{7}Be surface air concentrations, suggesting that the model adequately simulates the transport of ^{7}Be and ^{10}Be, even if the absolute magnitudes of the airborne isotopes are biased low.

4. Comparison With ^{10}Be Ice-Core Records

[12] In this section, we compare ice-core data from Dye 3 [*Beer et al.*, 1990] and South Pole [*Raisbeck et al.*, 1990], and firn-core data from Taylor Dome [*Steig et al.*, 1996], with data from the corresponding model gridboxes. Since the observations are given in terms of ^{10}Be snow concentration, we calculate the modeled snow concentration values from the simulated snowfall in water equivalent terms and ^{10}Be deposition output. Table 1 compares observed and modeled snow concentrations at each of the three locations, averaged over the years covered by the observations (1900–1984 for Dye 3, 1922–1994 for Taylor Dome, and 1906–1982 for South Pole). The three data sets collectively cover nearly all of the 20th century, however their overlap period is smaller, spanning the 60 years from 1922–1982. The time resolutions for the three time series also vary: observations at Dye 3 are given on an annual basis, while at Taylor Dome observations are given approximately every 2–3 years, and at South Pole approximately every 6–10 years.

[13] Unlike the general bias toward low model concentrations discussed in the previous section, the modeled ^{10}Be snow concentrations at Dye 3 and Taylor Dome are both very close to but slightly higher than the observed values. At South Pole, however, the simulated concentrations are significantly higher than the observations. While the tendency toward high snow concentrations at South Pole was also the case in earlier work with ModelE [*Field et al.*, 2006], the opposite is the case with the ^{7}Be surface air concentrations discussed in the preceding section: 1.52 mBq/SCM in the model vs. 4.21 mBq/SCM in the observations. The fact that the snow concentrations are high (despite the relatively low surface air concentrations) is mainly because of insufficient snow accumulation in the model. At South Pole, the average 20th century snow accumulation is approximately 1.8 cm/yr, lower than the observations, which range from approx. 5 cm/yr to approx. 10 cm/yr [*Bromwich*, 1988; *Mosley-Thompson et al.*, 1999; *Monaghan et al.*, 2006; *van der Veen et al.*, 1999] (all accumulation values are in water equivalent units). Model performance is better at the other two locations: the average simulated accumulation at Dye 3 is about 60 cm/yr, in good agreement with the 56 cm/yr estimate based on data from 1979–1981 [*Vinther et al.*, 2006] and with the 45 cm/yr estimate based on data from 1976–1997 at North Dye 3 nearby [*Mosley-Thompson et al.*, 2001]. At Taylor Dome, the model average is about 16 cm/yr, larger than the approx. 1–12 cm/yr estimate based onground measurements from 1992–1996 [*Morse et al.*, 1999] and the approx. 7 cm/yr based on firn-core estimates from 1954–1964 [*Steig et al.*, 1998], but more comparable to the approx. 12–14 cm/yr estimate based on satellite data [*Morse et al.*, 1999]. Additional discussion of the model climatology can be found in the work of *Field et al.* [2006] and *Field et al.* [2009].

[14] Here we normalize our results and the observations by the long-term average value for each location in order to illustrate the nature of the changes more robustly. Figure 4 shows ^{10}Be snow concentration over time at the three locations. The plots show the five-run average for the model runs with the full set of climate forcings, as well as the minimum and maximum simulated values from the ensemble (results for the simulations with SST forcing only were very similar and are not shown here). For Dye 3, the observations and model results are smoothed with a 3-point binomial filter. For Taylor Dome and South Pole, the modeled data have been averaged over the same time intervals as those inferred for the observations. In Figure 4 (top), the blue line shows the ϕ values used in these simulations. The ϕ values have been normalized in the same way as the ^{10}Be snow concentrations (by dividing each ϕ value by the 20th century average value) and inverted to clarify the similarity between the trend in ϕ and the trend in ^{10}Be concentration. It is important to note that these ϕ are not equivalent to expected ^{10}Be snow concentration values and are only meant to be indicative of the general forcing.

[15] Figure 4 (top) also shows the years of observed solar minima and maxima, according to international sunspot counts: each plus and minus symbol marks the year after the observed sunspot maxima and minima (respectively), in order to account for ^{10}Be's approximate 1-year atmospheric residence time. The minima and maxima indicated here do not necessarily occur simultaneously with the years of minimum and maximum ϕ values, however they provide a qualitative indication of when those production changes occurred. Table 2 also shows the minimum and maximum values for both the model data and the observations at each core site.

[16] The five-run averages can be considered an estimate of the expected climatological depiction of changes in ^{10}Be snow concentration, while the observations are most analogous to the results of a single model run. We would therefore hope that the observations fall within the envelope of the minimum and maximum simulated values. Despite some small excursions, this is largely the case for Dye 3. The 11-year solar signal is also visible for most of the record (though somewhat less so from about 1930–1950) and the associated peaks and troughs in the simulated ^{10}Be generally correspond well with those in the observations. There is also a similar agreement between the applied ϕ values and the observed and modeled ^{10}Be snow concentrations.

[17] In the plot for Taylor Dome, the model's aforementioned tendency toward lower levels of high-latitude variability is more apparent, with the observations extending

both above and below the envelope of the maximum/minimum values at several points in the record. This smaller range of simulated variability can also be seen in the differences in amplitude between the model and observations for sunspot minima (for instance, the minimum around 1977) and maxima (around 1980). Another characteristic of the Taylor Dome record is that the model's production-related peaks and troughs sometimes lag slightly behind the observations, such as around 1934 and 1971, however we note that some uncertainty in the timescales cannot be excluded. This lag may also be partially caused by the local increase in production because of low-energy solar particles during the descending limb of the solar cycle [*Koch and Mann*, 1996].

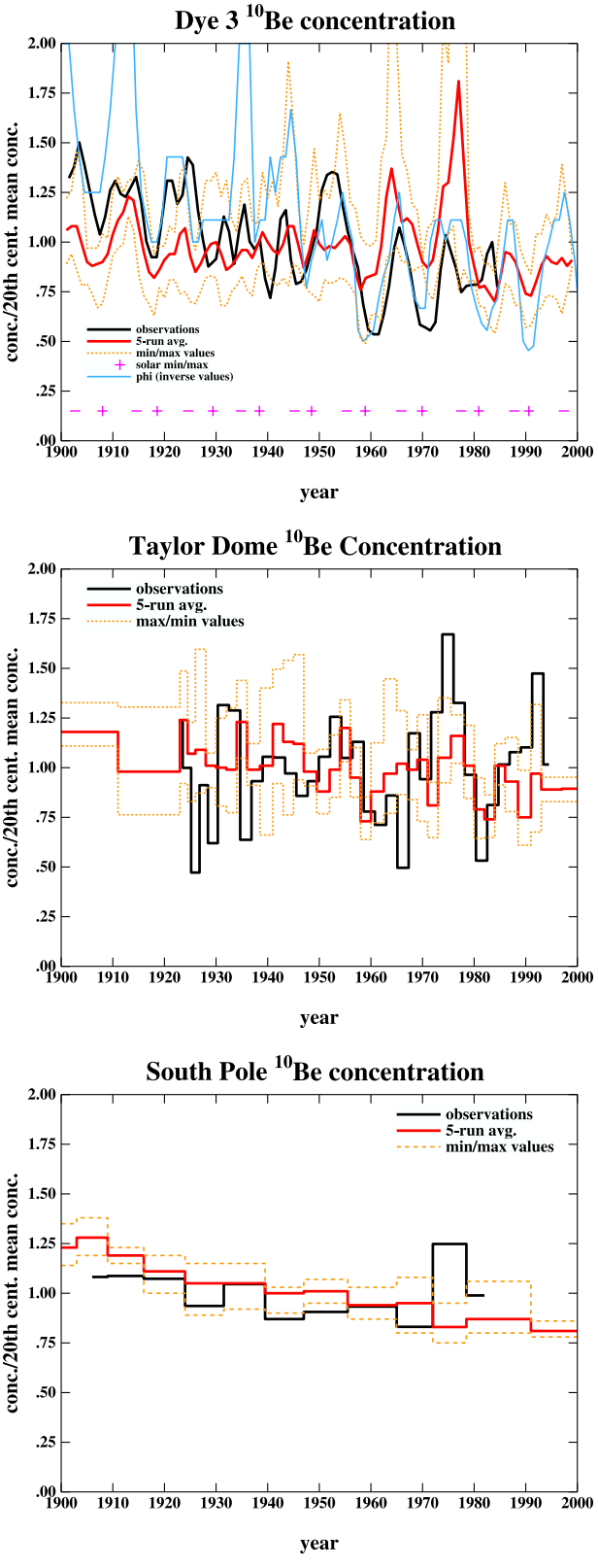

[18] The data for South Pole are characterized by a somewhat different set of features than those at Dye 3 and Taylor Dome, due perhaps to the lower number of observations. As a result, the 11-year solar cycle is obscured at South Pole compared with the data at the other two locations. The downward trend in the simulated South Pole ^{10}Be is stronger than in the observed values, however for the most part the observations fall within the maximum/minimum envelope of the model results. The main exception to this is the large peak in the observations corresponding to the solar minimum around 1977. This feature is also quite pronounced in the Taylor Dome observations but less so at Dye 3, suggesting that anomalous regional weather conditions (for instance, low snowfall over Antarctica, but average conditions over Greenland) might have played a role at this and other points in the ice-core record.

[19] As mentioned earlier, we have focused our discussion on ^{10}Be snow concentration since these are the values directly measured from the ice cores. While it is also possible to discuss ^{10}Be changes in terms of total deposition, this approach is not necessarily advantageous since it requires making estimates of the accumulations rates in the different ice cores and introduces added uncertainties. Furthermore, even if the accumulation rates could be estimated accurately, that would not ensure that the resulting ^{10}Be deposition rate data provide a better indication of solar-related production changes, since ^{10}Be deposition, like snow concentrations, can also be influenced by climate-related factors [*Field et al.*, 2006; *Alley et al.*, 1995]. With that in mind, we show modeled ensemble-mean snow accumulation, ^{10}Be deposition and snow concentration values in Figures 5, 6, and 7, to provide a qualitative idea of how accumulation and ^{10}Be deposition impact the simulated snow concentration values. Figure 5 shows downward trends in ^{10}Be deposition that are very similar over time at all three locations, in keeping with the applied ϕ forcing shown in Figure 1. The alternating high and low values in the deposition data also correspond respectively with the low and high ϕ values associated with the 11-year sunspot cycle.

[20] However, trends in snow accumulation rates vary from site to site (Figure 6). At Dye 3, the downward trend in ^{10}Be snow concentration is largely caused by the downward trend in ^{10}Be deposition, despite variable accumulation

Figure 4. Observed ^{10}Be snow concentrations (black line) and the five-run modeled ensemble average concentrations (red line). The dotted orange lines show the minimum and maximum values over time for each ensemble. The blue line in the top shows inverse ϕ values, normalized by the 20th century average value (note that this is not scaled to suggest an "expected" concentration value). The pink plus and minus symbols in the top denote the years of solar maxima and minima respectively, based on international sunspot counts.

Table 2. Normalized Minimum and Maximum ^{10}Be Snow Concentrations Over the 20th Century[a]

Location	Observed Minimum	Observed Maximum	Modeled Minimum	Modeled Maximum
Dye 3	0.54	1.50	0.49	4.99
Taylor Dome	0.47	1.67	0.68	1.44
South Pole	0.87	1.25	0.75	1.38

[a]Modeled values show the minimum and maximum values for the ensemble with the full set of forcings.

rates. Accumulation plays a more significant role at Taylor Dome, where ^{10}Be snow concentration values more closely resemble the accumulation rate time series. At South Pole, *Mosley-Thompson et al.* [1999] observed increases in snow accumulation from between 1965 and 1999. In the modeled South Pole data, there is a century-long upward trend in accumulation (approximately a 20% increase between 1900 and 2000), and also a downward trend in ^{10}Be deposition, both of which contribute to the negative trend in ^{10}Be snow concentration at that location. At Dye 3 and Taylor Dome, the minimum and maximum accumulation values for the different ensemble members range between 50% smaller or larger than the ensemble mean value; at South Pole, the variability is somewhat smaller, ranging from approximately ±30% of the ensemble mean value.

[21] Figure 7 shows what the modeled ^{10}Be snow concentration would look like at the three sites if ^{10}Be deposition were constant. (If snow accumulation rates were constant, we would obtain the snow concentration values by dividing the total deposition values by a constant number, and therefore the curve for the modeled ^{10}Be snow concentration would be the same as that in Figure 5).

[22] Figures 5, 6, and 7 demonstrate that while modeled ^{10}Be deposition provides a robust representation of the production signal in these experiments, this production signal can be obscured by local snow accumulation changes, which can impact ^{10}Be snow concentrations to a considerable extent. In providing an opportunity to study plausible representations of the 20th century ^{10}Be record, our simulations show that snow accumulation values need to be taken into account when one is trying to infer ^{10}Be production changes from ice-core data, and as noted earlier, determining snow accumulation rates is rarely a straightforward matter.

[23] In order to examine the coherence of the different ^{10}Be records over different timescales, for each ensemble member we correlated the ^{10}Be snow concentration time series between locations; we then smoothed the records with a 3-point binomial filter and correlated them a second time; then we repeated the process and correlated them a third time. Taylor Dome and South Pole were the only pair of locations for which all ensemble members were significantly correlated without smoothing, implying that relative proximity between ice cores leads to better correlation. For Dye 3/Taylor Dome and Dye3/South Pole, the high correlation values for some ensemble members do increase when successive filters are applied. However, for these multidecadal timescales, we do not see a notable increase in the significance of the correlation for the lower values as a result of smoothing (or successive smoothing). We take this to indicate that smoothing does not necessarily lead to a considerable improvement in the correlation of snow concentration records from different locations, at least over the course of the 20th century.

5. Trends in ^{10}Be Snow Concentration

[24] Figure 8 shows the percent change in ^{10}Be snow concentration per decade at the ice-core locations with

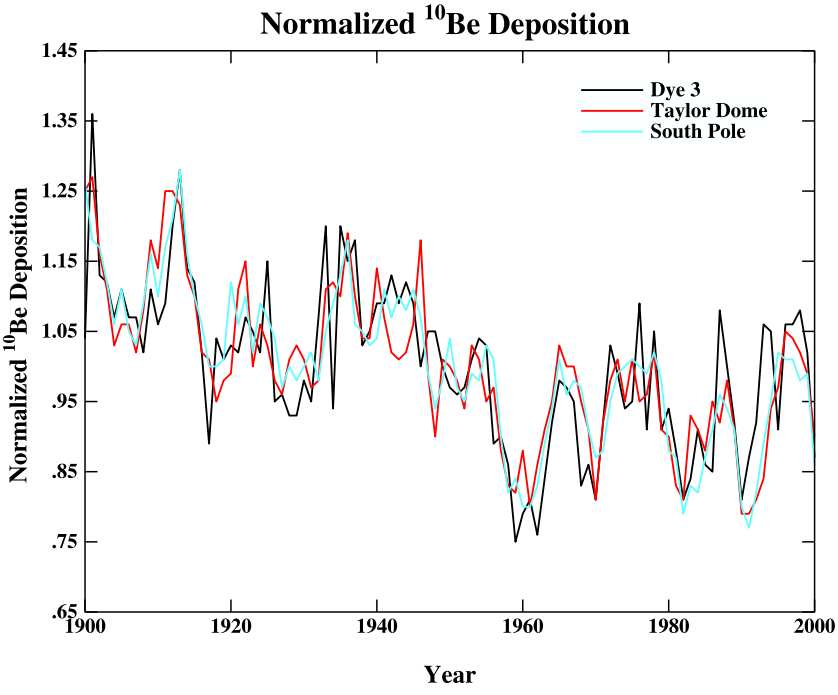

Figure 5. Total modeled ^{10}Be deposition, normalized by the 20th century average value at each location.

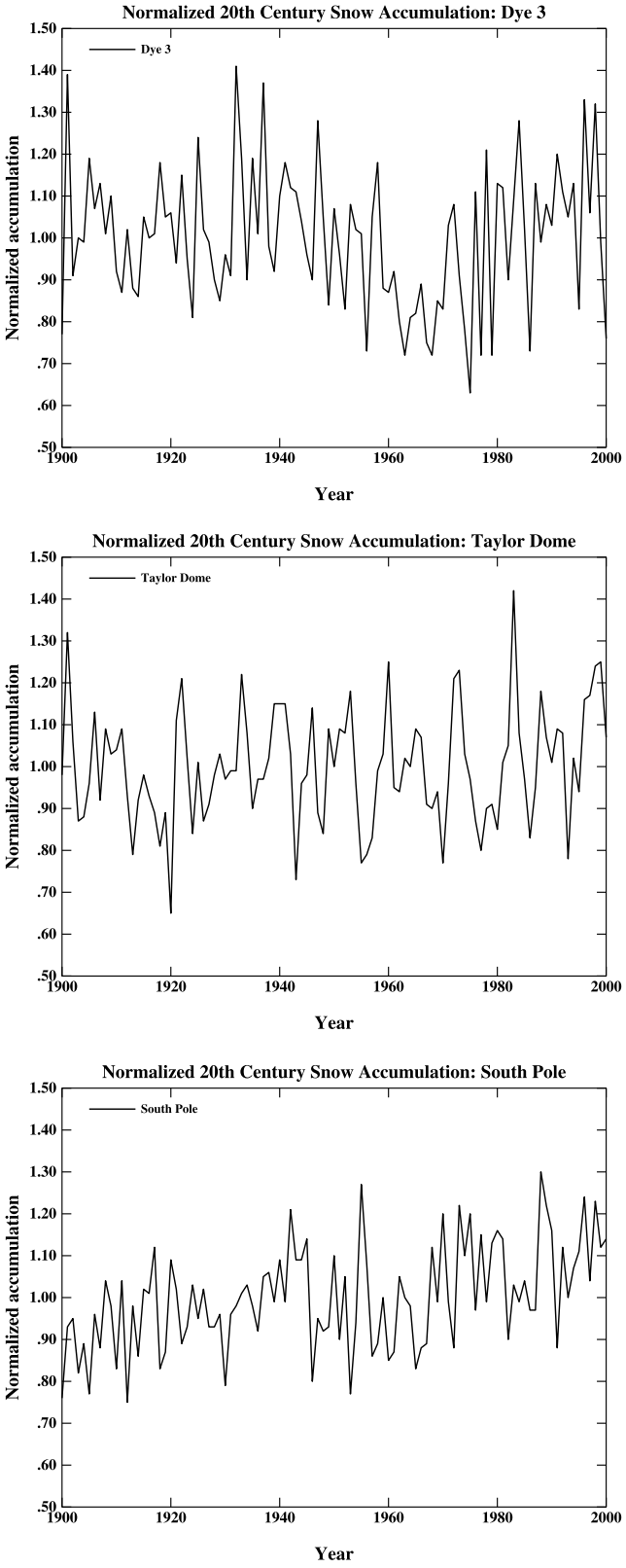

Figure 6. Modeled snow accumulation at the three core sites, normalized by the 20th century average value at each location.

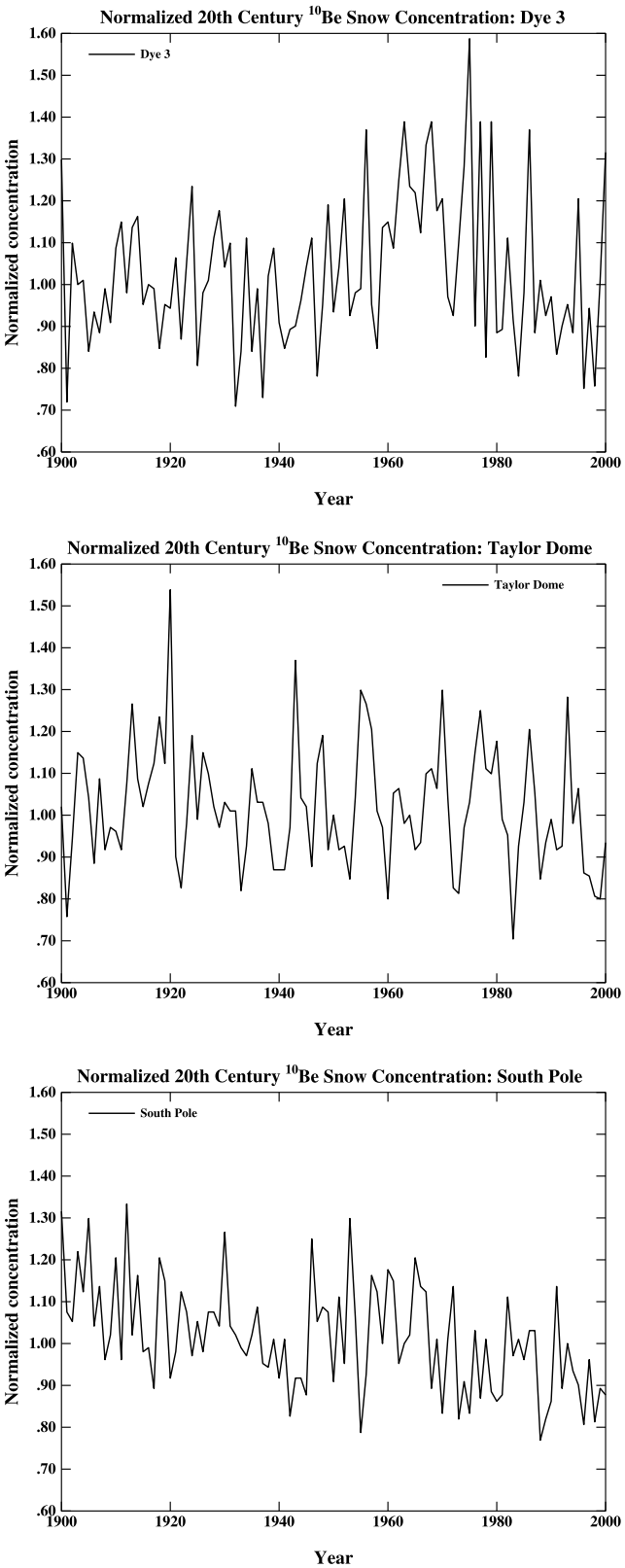

Figure 7. Modeled ^{10}Be snow concentration at the three core sites (for the hypothetical case of constant ^{10}Be deposition) normalized by the 20th century average value at each location.

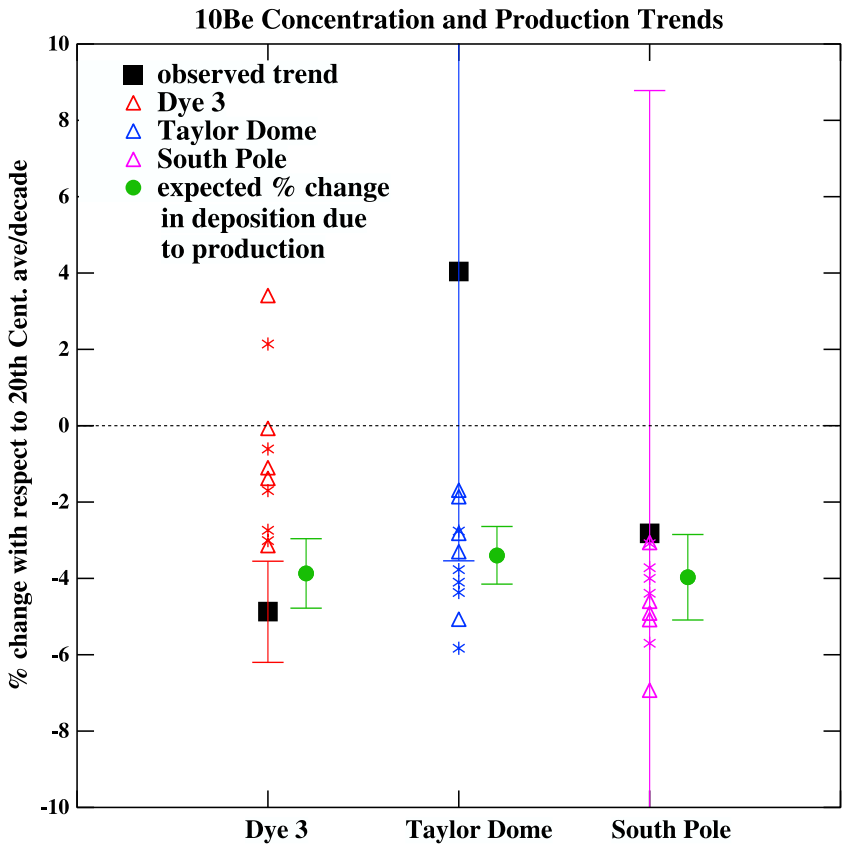

Figure 8. Trends in the 20th century ^{10}Be snow concentration and production. Black squares show the trend in the observed ^{10}Be concentrations (data from *Beer et al.* [1990] for Dye 3, *Steig et al.* [1996] for Taylor Dome, and *Raisbeck et al.* [1990] for South Pole). The colored triangles (ensemble members with all forcings) and stars (ensemble members with SST forcing only) show the trends in modeled ^{10}Be concentration. The green circles show the expected percent change in total ^{10}Be deposition at each location based on the changes in ^{10}Be production (ϕ) and the expected polar enhancement. All confidence intervals cover two standard deviations.

respect to the 20th century average values. Since the results for both the ensemble with SST forcing only and the ensemble with the complete set of forcings are so similar to each other, we combine all ten ensemble members to calculate the average modeled 20th century trends shown in Table 3. The green circles in Figure 8 also show the expected percent change in ^{10}Be deposition at each location based on the years covered by the observations. We calculated these expected deposition changes from the trends in ^{10}Be production, which were forced by the ϕ values shown in Figure 1. Previous work has shown that because of the increased levels of ^{10}Be production at high latitudes, when ϕ is reduced, global average production increases; however, a greater increase in ^{10}Be deposition takes place at latitudes higher than 60° [*Field et al.*, 2006]. This additional increase in high-latitude deposition is 20% above the global mean increase. Thus we calculated the trend in 20th century global average ^{10}Be production and increased that value by 20% to get the expected high-latitude deposition changes, shown by the green circles. The expected deposition changes at all locations agree with each other statistically, and all three fall within the uncertainties of the observed concentration trends. The expected deposition trends are slightly different because of the differences in time period relevant for each core.

[25] With the exception of two ensemble members at Dye 3, the modeled trends for all runs as well as the average trends at each location are negative, consistent with the changes in ϕ over the course of the century. However the fact that the observed trend at Taylor Dome is positive (though small) indicates the possibility that climate or weather variability can substantially alter the production signal, and that two records from the same ice sheet can have substantially different trends. (Although given the very large error bars on the trends at Taylor Dome and South Pole, the observed trends at all three locations agree with each other within two standard deviations.)

Table 3. Average Modeled Trends in ^{10}Be Snow Concentrations ±1 Standard Deviation[a]

Data Years	Dye 3 1900–1984	Taylor Dome 1922–1994	South Pole 1906–1982
Observations	−4.87 ± 1.33	4.04 ± 7.58	−2.82 ± 11.61
Model	−0.82 ± 1.42	−3.56 ± 1.42	−4.55 ± 1.03
Expected change from production alone	−3.87 ± 0.91	−3.40 ± 0.75	−3.97 ± 1.12

[a]Modeled values are averaged over both the runs with all forcing and the runs with SST forcing only. Units are in percent change per decade with respect to the 20th century average value.

[26] The modeled trends at the two Antarctic locations closely resemble each other both in terms of range and magnitude. Half of the trend values at Taylor Dome and all of the values at South Pole are in statistical agreement with their respective observed trends (again, however, the sizeable error bars at these two locations diminishes to some degree the robustness of this agreement). We also looked at the correlation between locations for all ten of the simulated trend values. Although trends at Taylor Dome and South Pole were somewhat more highly correlated with each other than with Dye 3, none of the trends at each site were significantly correlated, implying that much of the variance seen in the model results in Figure 8 is simply caused by internal unforced variability. These characteristics collectively illustrate that century-scale trends in modeled ^{10}Be snow concentration can be systematically different at different locations.

[27] For the more highly sampled Dye 3 record, none of the simulated concentration trend values fall within the error bars for the observations, and all are less negative than the observed trend. Also, the range of the simulated trends at this location is much greater than at Taylor Dome or South Pole. The size of the range of the trends for the modeled Dye 3 data and for the Antarctic locations suggest that, in the model, the impact of internal variability is larger at Dye 3. Although internal variability plays a smaller role at Taylor Dome and South Pole, the concentration trends for the individual ensemble members at those locations can vary by up to approximately 50% from the mean value.

[28] At least some if not most of the modeled trend values agree with the expected deposition trends at each location; however, at Dye 3, the average concentration trend is notably more positive than the expected production trend. Since climate change and production change are the only two factors affecting ^{10}Be snow concentration in these experiments (once weather is averaged out), we can infer that the difference between the mean modeled concentration trends and the expected production-related trend is caused by climate change. Figure 8 therefore shows that modeled climate effects at Dye 3 minimize the anticipated production change signal. As for Taylor Dome and South Pole, the greater overlap between the closely clustered trend values at these locations and their respective predicted deposition changes implies that modeled ^{10}Be snow concentrations at these locations are perhaps better proxies for changes in ϕ.

6. Conclusions

[29] We have shown that on interannual and decadal timescales, the relative variability of beryllium isotopes simulated with the GISS ModelE GCM agrees well with changes in observed surface air concentrations, despite the low bias of the modeled ^{7}Be in surface air with respect to the observations.

[30] In comparison with the ^{10}Be ice-core records, the model's internal variability is comparable to the inferred internal variability implied in the ice-core observations. It is somewhat more difficult to evaluate how well the model performs at South Pole because of the large sampling interval in the data and the poorly simulated accumulation rates. Improved time resolution in the ^{10}Be record at this location would be especially helpful in making further analysis. Model results suggest that during the 20th century geographical closeness seems to have a greater impact on correlation than does the use of smoothing functions, or successive smoothing.

[31] At Taylor Dome, the observations show that it is possible to get local trends in 20th century ^{10}Be concentration that are different from the trends suggested by changes in production based on the relatively well-constrained inferred ϕ values.

[32] The low levels of correlation between the modeled concentration trends at different locations suggest that internal unforced variability is the main cause for the differences in snow concentration trends from location to location. While internal variability affects all three locations, the relatively narrow range of modeled concentration trends at Taylor Dome and South Pole, and the good agreement between their concentration trends and the corresponding ϕ changes, suggest that, in the model at least, Antarctic locations are more accurate proxies for changes in cosmogenic isotope production on multidecadal timescales during the 20th century. The relatively broad range of simulated concentration trends at Dye 3 shows that climate changes at this site make it possible to get modeled trends in 20th century ^{10}Be snow concentration that are notably smaller in magnitude than what one would expect based on the applied changes in ϕ. However the fact that the observed concentration trend at Dye 3 is actually more negative than the production trend suggests that there are shortcomings in the way the model simulates ^{10}Be over southern Greenland, and perhaps over broader areas of the Greenland ice sheet as well. Since the 20th century climate forcings used here are relatively well constrained, it is more likely that the problem lies with the model itself. Future work with higher spatial resolution and improved model physics will allow us to further investigate these issues.

[33] Note: The simulated cosmogenic isotope data used in this article can be downloaded from www.giss.nasa.gov.

[34] **Acknowledgments.** We would very much like to thank to Jürg Beer for his many helpful comments and for supplying ^{10}Be and ^{7}Be production functions. Two anonymous reviewers also helped improve the manuscript substantially. Thanks to Raimund Muscheler for the reconstructed ϕ values, and to EML/SASP (http://www.eml.st.dhs.gov/databases/sasp/sasp_data_search.htm) for providing the ^{7}Be data. Support for this project was provided by NSF grant ATM-0317562. Christy Field also acknowledges support from the U.S. National Science Foundation through a Fellowship in the IGERT Joint Program in Applied Mathematics and Earth and Environmental Sciences at Columbia University.

References

Alley, R. B., R. C. Finkel, K. Nishiizumi, A. Anandakrishnan, C. A. Shuman, G. R. Mershon, G. A. Zielinski, and P. A. Mayewski (1995), Changes in continental sea-salt atmospheric loadings in central Greenland during the most recent deglaciation: Model based estimates, *J. Glaciol.*, *41*, 503–514.

Balkanski, Y. J., D. J. Jacob, G. M. Gardner, W. C. Graustein, and K. Turekian (1993), Transport and residence times of tropospheric aerosols inferred from a global three-dimensional simulation of ^{210}Pb, *J. Geophys. Res.*, *98*, 20,573–20,586.

Bard, E., G. M. Raisbeck, F. Yiou, and J. Jouzel (1997), Solar modulation of cosmogenic nuclide production over the last millennium: Comparison between ^{14}C and ^{10}Be records, *Earth Planet. Sci. Lett.*, *150*, 453–462.

Bard, E., J. Jouzel, and G. M. Raisbeck (2007), Comment on "Solar activity during the last 1000 yr inferred from radionuclide records" by Muscheler et al. (2007), *Quat. Sci. Rev.*, *26*, 2301–2304.

Beer, J. (2000), Neutron monitor records in broader historical context, *Space Sci. Rev.*, *93*, 107–119.

Beer, J., et al. (1990), Use of ^{10}Be in polar ice to trace the 11-year cycle of solar activity, *Nature*, *347*, 164–166.

Bromwich, D. H. (1988), Snowfall in high southern latitudes, *Rev. Geophys.*, *206*, 149–168.

Chin, M., D. J. Jacob, G. M. Gardner, M. S. Foreman-Flower, P. A. Spiro, and D. L. Savoie (1996), A global three-dimensional model of tropospheric sulfate, *J. Geophys. Res.*, *101*, 18,667–18,690.

Field, C. V., G. A. Schmidt, D. Koch, and C. Salyk (2006), Modeling production and climate-related impacts on ^{10}Be concentration in ice cores, *J. Geophys. Res.*, *111*, D15107, doi:10.1029/2005JD006410.

Field, C. V., G. A. Schmidt, and D. T. Shindell (2009), Interpreting ^{10}Be changes during the Maunder minimum, *J. Geophys. Res.*, *114*, D02113, doi:10.1029/2008JD010578.

Gleeson, L. J., and W. I. Axford (1968), Solar modulation of galactic cosmic rays, *Astrophys. J.*, *154*, 1011–1018.

Heikkilä, U., J. Beer, and J. Feichter (2008), Modeling cosmogenic radionuclides ^{10}Be and ^{7}Be during the Maunder minimum using the ECHAM5-HAM general circulation model, *Atmos. Chem. Phys.*, *7*, 2797–2809.

Hicks, B. B., D. R. Matt, and R. T. McMillen (1989), A micrometeorological investigation of surface exchange of O_3, SO_2 and NO_2: A case study, *Boundary Layer Meteorol.*, *47*, 321–336.

Koch, D. M., and D. Rind (1998), Beryllium 10/beryllium 7 as a tracer of stratospheric transport, *J. Geophys. Res.*, *103*, 3907–3917.

Koch, D. M., and M. E. Mann (1996), Spatial and temporal variability of ^{7}Be surface concentrations, *Tellus*, *48B*, 387–396.

Koch, D., G. A. Schmidt, and C. Field (2006), Sulfur, sea salt and radionuclide aerosols in GISS modelE, *J. Geophys. Res.*, *111*, D06206, doi:10.1029/2004JD005550.

Lal, D., and B. Peters (1967), Cosmic ray produced radioactivity on the Earth, *Handb. Phys.*, *46*, 551–612.

Lean, J. (1994), Solar forcing of global change, in *The Solar Engine and its Influence on Terrestrial Atmosphere and Climate*, *NATO ASI Ser.*, vol. 25, pp. 163–184, Springer, Berlin.

Lean, J. L., Y.-M. Wang, and J. N. R. Sheeley (2002), The effect of increasing solar activity on the Sun's total and open magnetic flux during multiple cycles: Implications for solar forcing of climate, *Geophys. Res. Lett.*, *29*(24), 2224, doi:10.1029/2002GL015880.

Masarik, J., and J. Beer (1999), Simulation of particle fluxes and cosmogenic nuclide production in the Earth's atmosphere, *J. Geophys. Res.*, *104*, 12,099–12,111.

Masarik, J., and R. C. Reedy (1995), Terrestrial cosmogenic-nuclide production systematic calculated from numerical simulations, *Earth Planet. Sci. Lett.*, *136*, 381–395.

McCracken, K. G., and B. Heikkila (2003), The cosmic ray intensity between 1933 and 1965, in *Proc. 28th Int. Cosmic Ray Conf.*, edited by T. Kajita et al., pp. 4117–4120, Univ. Acad. Press, Tokyo.

Monaghan, A. J., et al. (2006), Insignificant change in Antarctic snowfall since the International Geophysical Year, *Science*, *313*, doi:10.1126/science.1128,243.

Morse, D. L., E. D. Waddington, H.-P. Marshall, T. A. Neumann, E. J. Steig, J. E. Dibb, D. P. Winebrenner, and R. J. Arthern (1999), Accumulation rate measurements at Taylor Dome, east Antarctica: Techniques and strategies for mass balance measurements in polar environments, *Geogr. Ann. Ser. A*, *81*, 683–694.

Mosley-Thompson, E., J. F. Paskievitch, A. J. Gow, and L. G. Thompson (1999), Late 20th century increase in South Pole snow accumulation, *J. Geophys. Res.*, *104*, 3877–3886.

Mosley-Thompson, E., J. McConnell, R. Bales, Z. Li, P.-N. Lin, K. Steffen, L. Thompson, R. Edwards, and D. Bathke (2001), Local to regional-scale variability of annual net accumulation on the Greenland ice sheet from PARCA, *J. Geophys. Res.*, *106*, 33,839–33,851.

Mursula, K., I. G. Usoskin, and G. A. Kovaltsov (2003), Reconstructing the long-term cosmic ray intensity: Linear relations do not work, *Ann. Geophys.*, *21*, 863–867.

Muscheler, R., F. Joos, and J. Beer (2007a), Reply to the comment by Bard et al. on "Solar activity during the last 1000 yr inferred from radionuclide records", *Quat. Sci. Rev.*, *26*, 2304–2308.

Muscheler, R., F. Joos, J. Beer, S. A. Muller, M. Vonmoos, and I. Snowball (2007b), Solar activity during the last 1000 yr inferred from radionuclide records, *Quat. Sci. Rev.*, *26*, doi:10.1016/j.quascirev.2006.07.012.

O'Brien, K., H. A. Sandmeier, G. E. Hansen, and J. E. Campbell (1978), Cosmic-ray induced neutron background sources and fluxes for geometries of air over water, ground, iron, and aluminum, *J. Geophys. Res.*, *83*, 114–120.

Oeschger, H., J. Houtermann, H. Loosli, and M. Wahlen (1969), The constancy of cosmic radiation from isotope studies in meteorites and on the Earth, in *Radiocarbon Variations and Absolute Chronology*, edited by I. Olsen, 652 pp., John Wiley, New York.

Raisbeck, G. M., F. Yiou, J. Jouzel, J. R. Petit, N. O. Weiss, J. Alsop, and G. de Q. Robin (1990), ^{10}Be and δ^2H in polar ice cores as a probe of the solar variability's influence on climate, *Philos. Trans. R. Soc.*, *330*, 463–470.

Rind, D., J. Lerner, J. Jonas, and C. McLinden (2007), Effects of resolution and model physics on tracer transports in the NASA Goddard Institute for Space Studies general circulation models, *J. Geophys. Res.*, *112*, D09315, doi:10.1029/2006JD007476.

Schmidt, G. A., et al. (2006), Present day atmospheric simulations using GISS Model-E: Comparison to in-situ, satellite and reanalysis data, *J. Clim.*, *19*, 153–192, doi:10.1175/JCLI3612.1.

Shindell, D. T., G. Faluvegi, R. L. Miller, G. A. Schmidt, J. E. Hansen, and S. Sun (2006a), Solar and anthropogenic forcing of tropical hydrology, *Geophys. Res. Lett.*, *33*, L24706, doi:10.1029/2006GL027468.

Shindell, D. T., G. Faluvegi, N. Unger, E. Aguilar, G. A. Schmidt, D. M. Koch, S. E. Bauer, and R. L. Miller (2006b), Simulations of preindustrial, present-day, and 2100 conditions in the NASA GISS composition and climate model G-PUCCINI, *Atmos. Chem. Phys.*, *6*, 4427–4459.

Steig, E. J., P. J. Polissar, M. Stuiver, P. M. Grootes, and R. C. Finkel (1996), Large amplitude solar modulation cycles of ^{10}Be in Antarctica: Implications for atmospheric mixing processes and interpretation of the ice core record, *Geophys. Res. Lett.*, *23*, 523–526.

Steig, E. J., D. L. Morse, E. D. Washington, and P. J. Polissar (1998), Using the sunspot cycle to date ice cores, *Geophys. Res. Lett.*, *25*, 163–166.

Usoskin, I. G., and G. A. Kovaltsov (2008), Production of cosmogenic ^{7}Be isotope in the atmosphere: Full 3-D modeling, *J. Geophys. Res.*, *113*, D12107, doi:10.1029/2007JD009725.

van der Veen, C. J., E. Mosley-Thompson, A. J. Gow, and B. G. Mark (1999), Accumulation at South Pole: Comparison of two 900-year records, *J. Geophys. Res.*, *104*, 31,067–31,076.

Vinther, B. M., et al. (2006), A synchronized dating of three Greenland ice cores throughout the Holocene, *J. Geophys. Res.*, *111*, D13102, doi:10.1029/2005JD006921.

Vonmoos, M., J. Beer, and R. Muscheler (2006), Large variations in Holocene solar activity: Constraints from ^{10}Be in the Greenland ice core project ice core, *J. Geophys. Res.*, *111*, A10105, doi:10.1029/2005JA011500.

Wesely, M. L. (1989), Parameterization of surface resistances to gaseous dry deposition in regional-scale numerical models, *Atmos. Environ.*, *23*, 1293–1304.

Wesely, M. L., and B. B. Hicks (1977), Some factors that affect the deposition rates of sulfur dioxide and similar gases on vegetation, *J. Air Pollut. Control Assoc.*, *27*, 1110–1116.

Wesely, M. L., D. R. Cook, R. L. Hart, and R. E. Speer (1985), Measurements and parameterization of particulate sulfur dry deposition over grass, *J. Geophys. Res.*, *90*, 2131–2143.

Yang, S., H. Odah, and J. Shaw (2000), Variations in the geomagnetic dipole moment over the last 12000 years, *Geophys. J. Int.*, *140*, 158–162.

C. V. Field and G. A. Schmidt, NASA Goddard Institute for Space Studies, 2880 Broadway, New York, NY 10025, USA. (cfield@giss.nasa.gov)